AIP | Journal of Applied Physics

Space charge limited electron flow in two dimensions without magnetic field

A. Rokhlenko and J. L. Lebowitz

Citation: J. Appl. Phys. **110**, 033306 (2011); doi: 10.1063/1.3622152
View online: http://dx.doi.org/10.1063/1.3622152
View Table of Contents: http://jap.aip.org/resource/1/JAPIAU/v110/i3
Published by the American Institute of Physics.

Space charge limited electron flow in two dimensions without magnetic field

A. Rokhlenko[a] and J. L. Lebowitz[b]
Department of Mathematics, Rutgers University, Piscataway, New Jersey 08854-8019, USA

(Received 20 May 2011; accepted 30 June 2011; published online 10 August 2011)

We present a semi-analytic study of space charge limited electron flow from spatially periodic field emitters in the absence of a magnetic field. This extends our previous works, in which we assumed the existence of a strong magnetic field guiding the flow. We find that, in spite of the non-uniformity of the current density in the flow direction, the total current is very close to that obtained with a strong magnetic field in the same geometry and applied voltage. An analysis of the flow structure and comparison with the magnetized flow is given. © *2011 American Institute of Physics*. [doi:10.1063/1.3622152]

I. INTRODUCTION

Proper modeling of electron emission and space charge limited flow is very important for various applications, and there is an extensive literature studying it (see, for example, Refs. 1–18). In the pioneering works,[1] the flow was calculated under the assumption of infinite emissivity in flat, cylindrical, and spherical geometries. This analysis can be extended to other emission rules determining the relation between the emitter current density and the strength of the electric field at the cathode surface.[3,4] Using the symmetry of the flow, it is possible to compute the current density analytically, since the problem becomes essentially one-dimensional (1D) and can be reduced to an ordinary differential equation, albeit one with unusual boundary conditions (BC). The 1D approach can also be used as the basis of approximation schemes in other geometries. This was done in Refs. 5 and 6 using simple, but clever, modeling of the electric field created by a regular set of field emitters. Such approximations are necessary, because the analytic and even semi-analytic treatment of space charge limited (SCL) current in higher dimensions is extremely difficult mathematically, except in very special geometries.[7] In fact, most of the information about realistic flow geometries comes from numerical schemes, such as particle-in-cell simulations.[8–10]

One way to avoid the full complexity of higher dimensions is to consider situations in which there is a strong magnetic field guiding the flow of electrons. This was used by us in a series of works giving semi-analytic solutions in various geometries: in Ref. 11 for a narrow charged beam and in Ref. 12 for the planar 2D geometry with a finite emitting strip. There, we applied linearization techniques to obtain an approximate reduction of the full equation to an ordinary one. Similar situations were studied by several groups using numerical computational codes[8–10] (see also the review in Ref. 13). The simulations with and without the magnetic field for identical electrode geometries made in Ref. 9 led to the important observation that the total currents are quite close to each other in these cases. In practice, using a magnetic field in real devices (though being sometimes necessary) is in many situations clearly undesirable, because creating a strong field requires an additional energy source or heavy permanent magnets.

Here, we extend a least-square method developed in Refs. 14 and 15 for an approximate construction of the potential and current density for magnetized flows to the case where there is no magnetic field. We apply this method to the SCL flow from idealized periodic networks of field emitters with smooth analytic shapes in 2D. We compare the results with those of Ref. 14 for the magnetized flow and find closeness of average currents, in agreement with Ref. 9, though the distributions of the current density and electric field are different. Our analysis assumes the Fowler-Nordheim current-field emission law and is directed mainly to cases of metallic emitters and strong electric fields (but not so strong as to have to take into account new effects found in Ref. 16). We pay special attention to the effective electric fields at the emitter surfaces, which can be damaging for them and should therefore be monitored.

II. TWO-DIMENSIONAL PERIODIC SYSTEM OF EMITTERS

We use here the same setup as in Ref. 14, with long equidistant parallel ridges on the emitter surface and a flat anode. A cross-section of one half of an individual current bearing "cell" viewed along the y-axis is presented in Fig. 1.

The analytic form of the emitter in Fig. 1 is $u(x) = a(1-x^2)^2$, while the maximal anode-cathode distance is h. The ridge height a, as well as the applied anode voltage V, the emitter material, and distance h, will be variable parameters. Our idealized system is symmetric around $x=0$ and it is periodic on $-\infty < x < \infty$. The dimensionless units in Fig. 1 are defined below in Eq. (3).

Denoting by e, m the electron charge and mass, respectively, we have to solve the Poisson equation for the potential $\Phi(X,Z)$ and electron concentration $\rho(X,Z)$ in the stationary state

[a]Author to whom correspondence should be addressed. Electronic mail: rokhlenk@math.rutgers.edu.
[b]Also Department of Physics.

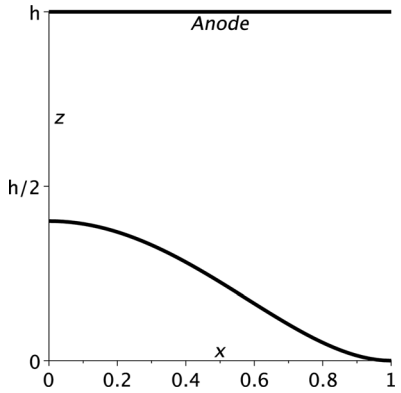

FIG. 1. x-z cross-section of a half-unit of the emitter-anode system.

$$\frac{\partial^2\Phi}{\partial X^2}+\frac{\partial^2\Phi}{\partial Z^2}=\frac{e}{\varepsilon_0}\rho(X,Z). \tag{1}$$

Eq. (1) is to be supplemented with the continuity equation for the current density $\vec{J}=e\rho\vec{v}$ (where $\vec{v}(X,Z)$ is the local electron velocity),

$$\nabla\vec{J}(X,Z)=0. \tag{2}$$

We use the usual[2,7] assumption that the electron flow is potential, i.e., the force acting on an individual electron is the gradient of a scalar function, Φ in our case. As the result, we have $m\frac{d\vec{v}}{dt}=e\vec{\nabla}\Phi$ and, therefore, $m[v^2(X,Z)-v_0^2]/2=-e\Phi$. Here, v_0 is the electron's initial velocity at the emitter surface. When considering strong electric fields, one can take $v_0=0$ and, thus, in Eq. (1), $e\rho=J\sqrt{m/2|e|}$.

The set of dimensionless variables and functions, which is used for computations and denoted by lower case letters, is the following:

$$X=xW,\ Z=zW,\Phi=\varphi V,\ J(X,Z)=\sqrt{\frac{2|e|}{m}}\frac{V^{3/2}}{W^2}\varepsilon_0 j(x,z), \tag{3}$$

where W is the physical half width of the cell, which corresponds to $x=1$ in Fig. 1, while hW is the maximal inter-electrode distance. In dimensionless units, Eq. (1) has the same form as in Refs. 4 and 11, but with the current density $j=\sqrt{j_x^2(x,z)+j_z^2(x,z)}$ dependent on both x and z:

$$\frac{\partial^2\varphi}{\partial x^2}+\frac{\partial^2\varphi}{\partial z^2}-\frac{j(x,z)}{\sqrt{\varphi(x,z)}}=0,\nabla\vec{j}(x,z)=0. \tag{4}$$

This makes the problem much more difficult than in the case of magnetized flow when $j=j(x)$.

The boundary conditions at the anode, cathode, and the vertical boundaries of the cell in Fig. 1 are

$$\varphi(x,h)=1,\varphi(x,u(x))=0,\frac{\partial\varphi}{\partial x}(0,z)=\frac{\partial\varphi}{\partial x}(1,z)=0,$$
$$j_n(x,u(x))\equiv j_n(x)=G[f_n(x,u(x))]. \tag{5}$$

Here, $f_n=\partial\varphi/\partial n$ is the electric field normal the emitter surface and $G(f)$ represents the Fowler-Nordheim current-field emission law[17]

$$G(f_n)=qf_n^2\exp(-p/f_n). \tag{6}$$

Values of q,p in Eq. (6) depend on the work function χ, voltage V, and the cell geometry. They depend also on the f_n, especially in strong fields, and we apply the results of Ref. 18 for modeling this dependence.

Without the magnetic field, the current density $\vec{j}$ is a vector given in terms of φ only at the cathode through j_n using Eqs. (5) and (6). Clearly, when $v_0=0$, the current densities and the electric fields at the cathode $z=u(x)$ are normal to the emitter surface and $j_n=|j|=\sqrt{j_x^2(x,u(x))+j_z^2(x,u(x))}$. Thus, there are additional BC for $\vec{j}$ at z $=u(x)$ (see Fig. 1),

$$j_x(x,u(x))=-\frac{j_n(x)u'}{\sqrt{1+(u')^2}},j_z(x,u(x))=\frac{j_n(x)}{\sqrt{1+(u')^2}}, \tag{7}$$

and due to the symmetry,

$$\frac{dj_x(x,z)}{dx}=\frac{dj_z(x,z)}{dx}=0\,\text{for}\,x=0,x=1,0<z<h. \tag{8}$$

III. METHOD OF SOLUTION

Our method of solving approximately this non-standard, nonlinear, boundary value problem is to construct its solution by choosing a set of trial functions with free parameters which describe the functions φ, j_x, and j_z and satisfy the BC. We determine the free parameters by minimizing the discrepancy in both equations in Eq. (4), i.e., including the divergence of the current $\nabla\vec{j}(x,z)$, on a representative set of points in the area bounded by $z=u(x),z=1,x=0$, and $x=1$. For doing this, the discrepancy and divergence in both equations in Eq. (4) are squared at each point and then summed over all chosen points. This gives two sums, and we minimize each of them in terms of the free parameters. For handling nonlinearity, we use iterations, i.e., the minimization at a given step does not include those parameters which are not present in the usual bilinear form, but corrected values of such parameters are substituted at the next step of iterations. The parameters of the current components, which enter in $\nabla\vec{j}(x,z)$ are optimized separately in alternation with the first functional, using their corrected values in it at the next step. The potential is modeled almost identically as in our paper:[14]

$$\varphi(x,z)=\varphi_0(x,z)+\sum_{i=1}^{N-2}c_{i+2}\varphi_i(x,z). \tag{9}$$

Here, the principal component $\varphi_0(x,z)$ of the potential is a solution of an algebraic equation representing the assumed equipotential surfaces

$$z=(1-\varphi_0)(1-c_1\varphi_0)u(x)+\varphi_0[h-c_2(1-\varphi_0)] \tag{10}$$

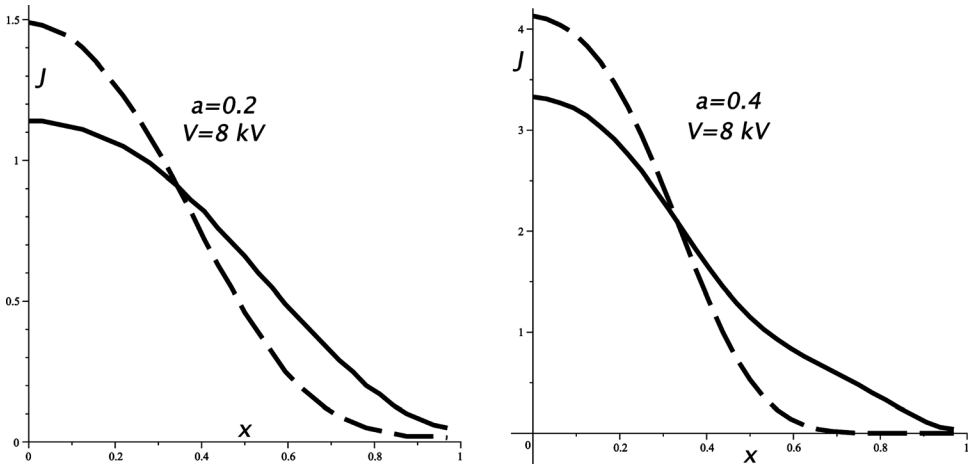

FIG. 2. The solid and broken lines give the value of $J(x)$ for the anode and cathode, respectively.

with two adjustable parameters, c_1 and c_2. For all other φ_i, we take algebraic functions with proper BC. The number of parameters N never exceeds 25. For the current density components, we use a set (not more than 12) of algebraic functions $(z-u)f_i, (z-u)g_k$ with free parameters r, s:

$$\begin{aligned} j_x(x,z) &= j_x(x) + [z-u(x)]\sum_i r_i f_i(x,z), \\ j_z(x,z) &= j_z(x) + [z-u(x)]\sum_k s_k g_k(x,z). \end{aligned} \tag{11}$$

Form (9) clearly satisfies BC (6), and f, g are chosen to satisfy Eq. (8). Using the least-square method and iterations, we evaluate r, s and the parameters of $c_1 \ldots c_N$. The total number of iterations for each set of entries (V, a, h) is usually around 100, and the process takes just a few computer seconds.

IV. CURRENT DENSITY PATTERN

Without the strong magnetic field, which makes the flow strictly vertical, the electrons spread out horizontally. This can substantially increase the current at values of x, where the cathode emission is very small. Fig. 2 illustrates this for a fixed anode voltage and two different heights of cathode bumps. The emitter has a period of $2W = 2$ microns, and the distance between the flat anode and the cathode valley is 1 micron ($h = 1$). The work function of the emitter material is taken to be 4.5 eV, which is typical for metals.

Unlike the strongly magnetized flows, the current density above the emitter tip $x = 0$ is decreasing along the z-axis, while for x closer to the valley (at $x = 1$), the current should grow when $z \to h$. This can be seen in Fig. 3, plotted for the same system as in Fig. 2.

In Figs. 2 and 3, the current densities are given in units of 10^8 Am/cm^2; they are quite high because the electric field strength at the emitter surface is large. We show in the next figure the distribution of the electric field $F(x)$, normal to the cathode surface, for three different ridge heights, keeping the other parameters the same.

One can see in Fig. 4 that, when a varies from 0.1 to 0.6, the maximum field at the top of the ridges increases only from 8 V/nm to 11 V/nm, i.e., by less than 40%, while the local inter-electrode distance decreases more than twice

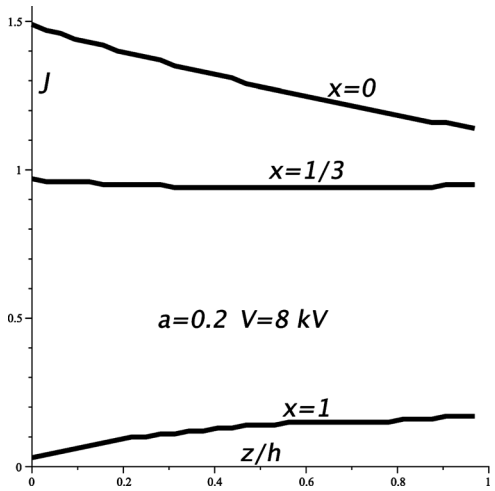

FIG. 3. Current density distribution along the z-axis for $x = 0, 1/3$, and 1.

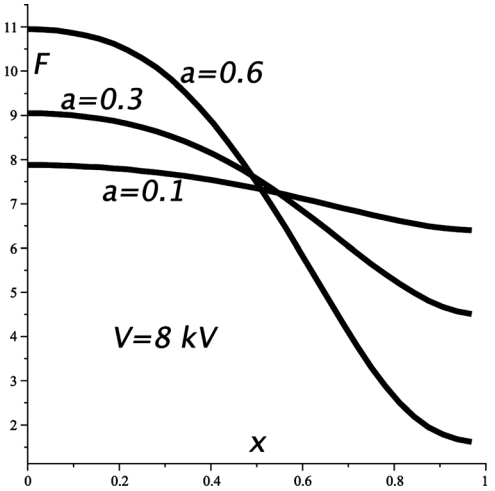

FIG. 4. Electric field strength at the cathode surface.

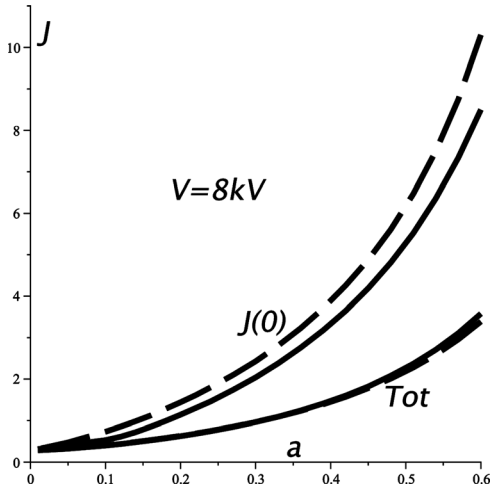

FIG. 5. Anode current densities $J(0)$ and total currents with and without magnetization.

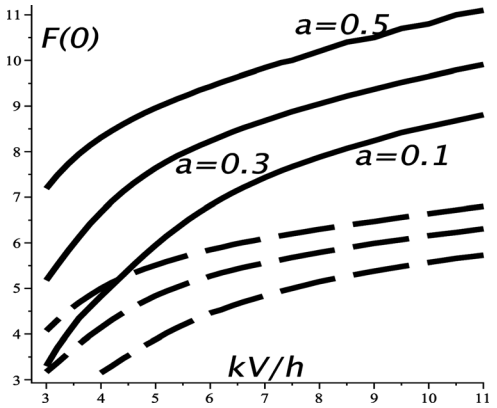

FIG. 7. Electric fields at the ridge top as functions of anode voltage for $h=1$ and $h=1.5$ (broken lines). When $h=1.5$, lines for $a=0.1, 0.3,$ and 0.5 are plotted in the same order as above, but vs $V \to 1.5\,V$.

from 0.9h to 0.4h. This is a result of screening by a much denser space charge when the tops of the ridges approach the anode.

In Fig. 5, we plot for $0.01 \leq a \leq 0.6$, the current densities at the ridge top J(0), and the total (Tot) currents for the present model and for the same geometry with a strong magnetic field. In the latter case,[14] the current density is independent of z at each x and determined by the cathode emission at the same point. Clearly, there is no necessity to minimize the current divergence in the computations of the magnetized flow.

The broken lines in Fig. 5 depict the flow in a very strong magnetic field directed along the z-axis. Though the total currents are almost the same for all values of a, the current density above the ridge top, $x=0$, is lower without the magnetic field, due to its spreading out. When $a \to 0$, the electron trajectories become parallel to the z-direction and have the same value for both cases. At the same time, the cathode emission at $x=0$ without magnetic field is stronger by $\sim 5\%$ when $a=0.3$ and $\sim 8\%$ for $a=0.6$ in this setup. This is caused by a more diluted space charge and lesser screening above the ridge top.

The behavior of the currents for the unmagnetized flow are exhibited in Fig. 6 as functions of the anode voltage with a fixed $a=0.3$ and, thus, for the same emitter curvature.

After increasing the inter-electrode distance and voltage by 50%, we nevertheless see a significantly lower current when $h=1.5$ as a result of stronger screening by the space charge. In both cases, the average anode and cathode currents are practically the same as they should be. This gives us confidence in the consistency of our computations. On the other hand, though the average currents strongly increase with V (see also Refs. 14 and 15 for the magnetized flow), the growth of the top anode currents slows down for larger V. We do not exclude that this is a result of loosing precision of our computations, but maybe this is a real effect of more intense flow spreading toward a diluted space charge when V increases.

The space charge effects on the normal to the cathode electric field can be clearly seen in Fig. 7, where the top $F(0)$ in V/nm is plotted as a function of the anode voltage for different values of a.

When $V=10\,\text{kV}$, the field intensities are 8.55 and 10.8 V/nm for $a=0.1$ and 0.5, respectively. Thus, they

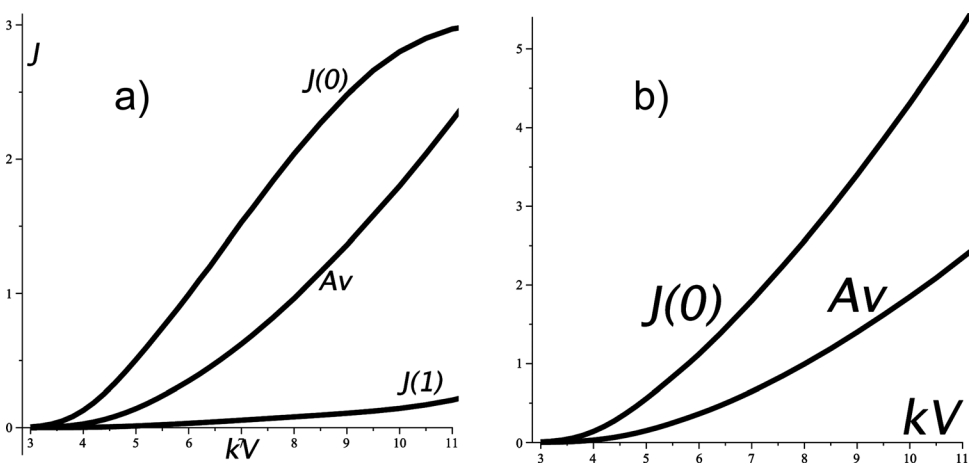

FIG. 6. a) Anode and b) cathode current densities. Symbol "Av" is for average current density.

differ by a factor of 1.26, while the local cathode-anode distance changes by a factor of $(1-0.1)/(1-0.5)=1.8$. The broken lines in Fig. 7 are for the case when the cell height is larger by 50%, and the anode voltages for plots are increased by the same factor for making similar cathode fields in vacuum. The larger h increases the screening effect, because the number of electrons between the electrodes is larger. In spite of correspondingly bigger V, the electric field, as well as the emission, are significantly weaker (see also Fig. 6).

V. CONCLUSION

Using a semi-analytic method, we calculated the electric field and current density pattern in a two-dimensional system consisting of a flat anode and a cathode-field emitter with a periodic set of smoothly shaped parallel ridges. Our results show that, as far as the total current is concerned, it is valid to assume the presence of a guiding strong magnetic field, which simplifies the computation and makes it more stable. Nevertheless, the distribution of the current density is quite different from the case of the magnetized flow. It is also likely that the absence of the steering forces will make the current unstable in some situations.

ACKNOWLEDGMENTS

We thank J. W. Luginsland for useful comments. Research supported by AFOSR Grant F49620-01-0154.

[1]C. D. Child, Phys. Rev. **32**, 492 (1911); I. Langmuir, *ibid* **2**, 450 (1913); I. Langmuir and K. B. Blodgett, *ibid* **22**, 347 (1923); I. Langmuir and K. B. Blodgett, *ibid* **24**, 49 (1924).
[2]M. Reiser, *Theory and Design of Charged Particle Beams* (Wiley, New York, 1994).
[3]R. G. Forbes, J. Appl. Phys. **104**, 084303 (2008).
[4]A. Rokhlenko, K. L. Jensen, and J. L. Lebowitz, J. Appl. Phys. **107**, 014904 (2010).
[5]K. L. Jensen, M. A. Kodis, R. A. Murphy, and E. G. Zaidman, J. Appl. Phys. **82**, 845 (1997).
[6]K. L. Jensen, J. Appl. Phys. **107**, 014905 (2010).
[7]A. Rokhlenko and J. L. Lebowitz, J. Appl. Phys. **102**, 123307 (2007).
[8]R. J. Umstattd and J. W. Luginsland, Phys. Rev. Lett. **87**, 145002 (2001).
[9]J. W. Luginsland, Y. Y. Lau, and R. M. Gilgenbach, Phys. Rev. Lett. **77**, 4668 (1996).
[10]Y. Feng and J. Verboncoeur, Phys. Plasmas **13**, 073105 (2006).
[11]A. Rokhlenko and J. L. Lebowitz, Phys. Plasmas **11**, 4559 (2004).
[12]A. Rokhlenko and J. L. Lebowitz, Phys. Rev. Lett. **91**, 085002 (2003).
[13]J. W. Luginsland, Y. Y. Lau, R. J. Umstattd, and J. J. Watrous, Phys. Plasmas **9**, 2371 (2002).
[14]A. Rokhlenko and J. L. Lebowitz, J. Appl. Phys. **107**, 103301 (2010).
[15]A. Rokhlenko and J. L. Lebowitz, J. Appl. Phys. **108**, 123301 (2010).
[16]A. Rokhlenko, J. Phys. A **44**, 055302 (2011).
[17]E. L. Murphy and R. H. Good, Phys. Rev. **102**, 1464 (1956).
[18]R. G. Forbes, Appl. Phys. Lett. **89**, 113122 (2006).